Cislunar Initial Orbit Determination with Optical Tracklets

John A Gaebler, Charles Wetterer, Keric Hill
KBR

ABSTRACT

A study is presented that characterizes the capabilities to initiate tracks for cislunar space objects. KBR is working toward standing up an end-to-end cislunar cataloging capability. One of the first steps in tracking a cislunar satellite is to find and establish a trajectory with an initial orbit determination (IOD) tool. KBR developed the Two Angle Pairs Initial Orbit with Conjunction Analysis (TAPIOCA) tool to perform IOD. For this effort TAPIOCA has been upgraded to find initial states of cislunar objects from optical tracks (right ascension and declination) produced by Electro-Optical ground-based sensors. Simulated data of multiple cislunar objects in various orbits are processed with the Space Catalog Observation Processing Engine (SCOPE). Care is taken to simulate a realistic scenario considering noise, scheduling, detection restrictions, etc., while including closely spaced objects and maneuvering objects. Results of establishing trajectories in a data rich environment are presented to illustrate a best-case scenario. Finally, simulation parameters are varied to stress the tool and provide insights into the capabilities and limitations.

1. INTRODUCTION

Interest in operating satellites in cislunar space has spiked in recent years, with multiple missions already flying. Due to the large distances and difficult sensor constraints, there is a need to upgrade passive tracking systems to achieve situational awareness throughout cislunar space. KBR is working toward standing up an end-to-end cislunar cataloging capability. One of the first steps in tracking a cislunar satellite is to find and establish a trajectory with an initial orbit determination (IOD) tool. Most classic IOD tools rely on two-body gravitational force model assumptions that can break down in cislunar space due to third-body gravitational effects of the Moon.

KBR developed the Two Angle Pairs Initial Orbit with Conjunction Analysis (TAPIOCA) tool to perform IOD, conjunction assessment with poorly determined orbits, and maneuver detection for traditional Earth orbits. For this effort TAPIOCA has been upgraded to find initial states of cislunar objects from optical tracks (right ascension and declination (RA/Dec)) produced by Electro-Optical ground- and space-based sensors. When observations of cislunar objects are processed with TAPIOCA, first an Earth-centric orbit is attempted, but if that fails TAPIOCA will attempt to establish a Lunar-centric orbit when certain conditions are met (the optical measurements are sufficiently close to the Moon sphere of influence). TAPIOCA still relies on two-body gravity assumptions, but over relatively short time scales, the initial two-body results are good enough to establish trajectories which can be refined with a batch least-squares algorithm using full force model predictions that include n-body dynamics. Note that many periodic orbits in the Earth-Moon three-body problem have periods of a week or more, so a short time scale relative to the orbit period can still be several hours. In the least-squares formulation, a singular-value decomposition solver is used to avoid numerical difficulties which occur for trajectories with poor observability.

KBR's end-to-end tool for managing a catalog is called the Space Catalog Observation Processing Engine (SCOPE). While the focus of this study is on the IOD capabilities applied to cislunar objects, a month-long simulation is analyzed to show that the IOD estimates are indeed good enough to seed a catalog. SCOPE is a robust tool that is tailored to handle any orbital regime, including cislunar scenarios. A brief high-level description of SCOPE will be provided in Section 2, along with a more detailed explanation of TAPIOCA.

While a simulation, attempts are made to mimic operational capabilities. Section 3 describes the high-fidelity test sets developed for this study. Observations are simulated with realistic scheduling constraints, measurement noise, and viewing restrictions. Objects are chosen to reside in high interest areas of cislunar space with truth trajectories created using a high-fidelity propagator. Special objects are also included to test the system against real world scenarios that could degrade system performance.

Section 4 presents the results of running SCOPE on the simulated data. The goal of the study is to test the strengths and weakness of the cislunar IOD capabilities in TAPIOCA. Most passive ground-based satellite surveillance systems are geared to track standard Earth orbiting satellites, from Low Earth to Geosynchronous regimes. Dedicated cislunar

Copyright © 2023 Advanced Maui Optical and Space Surveillance Technologies Conference (AMOS) – www.amostech.com

cataloging will likely require modified strategies, including IOD. As a starting point, this study focused on a parameter search of observation cadence, track length, and measurement noise. While testing the cataloging/IOD processes, these results will also help to guide the development and deployment of tracking systems dedicated to maintaining cislunar catalogs.

2. SOFTWARE BACKGROUND

2.1 SCOPE

SCOPE is a suite of software services in an open-loop configuration that ingests observation files and processes them chronologically in time steps. The services used in SCOPE are written in C++ and are also used operationally in a real-time processing configuration that is closed loop, meaning that the services dynamically task sensors based on events as they happen. The services can be distributed on a network and communicate via TCP/IP messages, many of which are binary serializations of C++ data structures. Astrodynamics calculations are performed using the Turboprop C++ astrodynamics library. Figure 1 shows the particular SCOPE configuration used for this study.

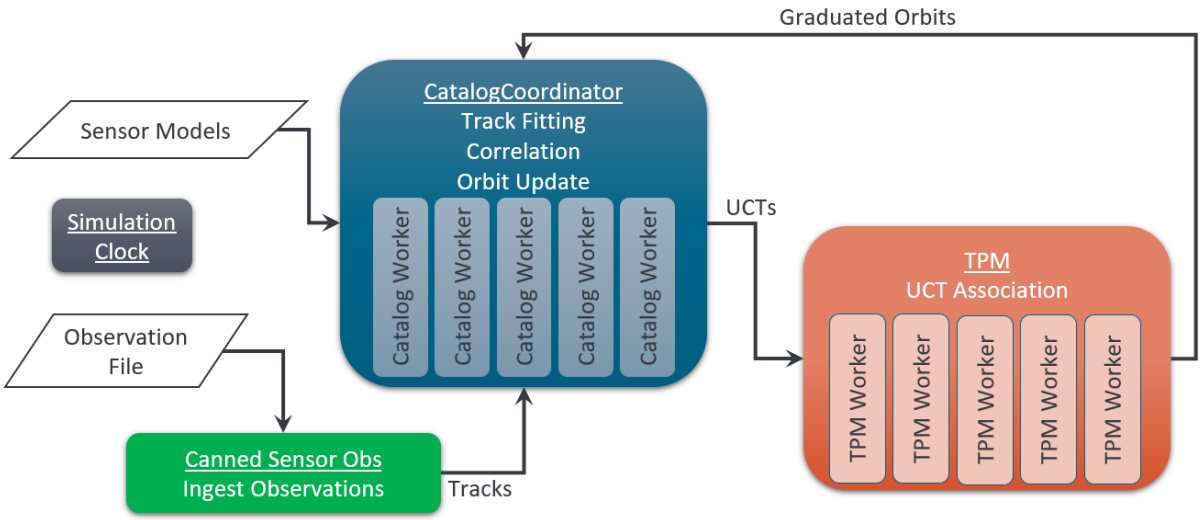

Figure 1: Schematic representation of the SCOPE configuration used for this paper.

The Simulation Clock steps through time, sending messages to the other services to notify them of the current time step. The other services notify the clock when they have completed all their tasks for the current time step, allowing the clock to advance the time.

The "Canned Sensor Obs" service reads a variety of observation file formats. If needed, observations are grouped into tracks. Sensor models including location, noise, and biases must be available for any observations ingested. Supported sensor types include optical, radar, and passive RF. Upon receiving a time step message, the sensor service sends any tracks ending in the current time step to the CatalogCoordinator service.

The space object catalog consists of many catalog worker services, each of which contains the Special Perturbations (SP) estimates, predictions, visibility, and observation history for a subset of all the catalog objects. The CatalogCoordinator service serves as a point of communication with other services, distributes requests to the catalog workers, and aggregates results. When tracks are received from the sensor service, CatalogCoordinator fits the observations in the track to an orbit or polynomial to produce refined angles and angle rates near the midpoint of the track time span. CatalogCoordinator sends the tracks and the fits to the workers and requests possible correlations (track-to-orbit associations). Based on the results the workers compute in parallel, CatalogCoordinator decides which correlation is the best and notifies the CatalogWorker storing that catalog object to update the orbit accordingly. If the track does not correlate to any catalog object, it is sent to the Tactical Persistent Monitoring (TPM) service for Uncorrelated Track (UCT) association.

Copyright © 2023 Advanced Maui Optical and Space Surveillance Technologies Conference (AMOS) – www.amostech.com

TPM attempts to associate UCTs and build new candidate orbits. Like the catalog, it has a TPM service which communicates with other services and coordinates computations done in parallel by the TPM workers. When a candidate orbit estimate reaches a required level of accuracy in predicted position uncertainty, it "graduates" and is sent to the catalog. CatalogCoordinator assigns a number to the graduated orbit and sends it to one of the catalog workers. Any future tracks for that object should correlate to the new estimate and be updated.

The output from SCOPE includes a log file detailing results of computations and a catalog file containing all the orbit and model estimates for the catalog objects, along with their observation history.

2.2 TAPIOCA

TPM uses a suite of C++ tools in Turboprop called TAPIOCA to associate tracks and perform IOD. Initially designed for optical tracks only, it has been upgraded to fuse optical, radar, and passive RF observations in the IOD process.

2.2.1 Track Reduction

Before associating tracks, it is necessary to compute a fit to the track and produce smoothed observations and their rates at the track midpoint. Optical tracks do not usually contain enough information to compute the complete orbit state of the object, and the behavior of the measurements over a short enough period of time can be approximated with a polynomial. For example, suppose there is a sorted list of m observations, Y_i, where $i = 1 \ldots m$, each with a measurement noise covariance matrix W_i. The measurements consist of the Right Ascension, α, and declination, δ, angles. The midpoint of the track is at time t_{mid}. The sequence of measurements can be fit to a quadratic using weighted least squares to produce a state vector, $\hat{Y}$, with a smoothed value for each measurement, $\alpha(t_{mid})$ and $\delta(t_{mid})$, their rates of change, $\dot{\alpha}$ and $\dot{\delta}$, and acceleration terms, $\ddot{\alpha}$ and $\ddot{\delta}$

$$\hat{Y} = [\alpha(t_{mid}) \quad \delta(t_{mid}) \quad \dot{\alpha} \quad \dot{\delta} \quad \ddot{\alpha} \quad \ddot{\delta}]^T . \tag{1}$$

The initial estimates for the angles and rates are created with the real observations at times t_1 and t_m,

$$\hat{Y}_0 = [\alpha(t_1) + \dot{\alpha}_0(t_{mid} - t_1) \quad \delta(t_1) + \dot{\delta}_0(t_{mid} - t_1) \quad \dot{\alpha}_0 \quad \dot{\delta}_0 \quad 0 \quad 0]^T \tag{2}$$

where

$$\dot{\alpha}_0 = \frac{\alpha(t_m) - \alpha(t_1)}{t_m - t_1} \tag{3}$$

$$\dot{\delta}_0 = \frac{\delta(t_m) - \delta(t_1)}{t_m - t_1} \tag{4}$$

and the initial accelerations are set to zero. Then residuals, y_i, are computed for each observation using the quadratic model:

$$y_i = Y_i - \begin{bmatrix} \alpha(t_{mid}) + \dot{\alpha}(t_i - t_{mid}) + \ddot{\alpha}(t_i - t_{mid})^2 \\ \delta(t_{mid}) + \dot{\delta}(t_i - t_{mid}) + \ddot{\delta}(t_i - t_{mid})^2 \end{bmatrix} \tag{5}$$

The new estimate for the augmented observation vector is

$$\hat{Y} = \left[\sum_{i=1}^{m} H_i^T W_i H_i\right]^{-1} \left[\sum_{i=1}^{m} H_i^T W_i y_i\right] + \hat{Y}_0 \tag{6}$$

where the relationship between the measured and estimated state is

Copyright © 2023 Advanced Maui Optical and Space Surveillance Technologies Conference (AMOS) – www.amostech.com

$$H_i = \frac{\partial Y_i}{\partial \hat{Y}} = \begin{bmatrix} 1 & 0 & t_i - t_{mid} & 0 & (t_i - t_{mid})^2 & 0 \\ 0 & 1 & 0 & t_i - t_{mid} & 0 & (t_i - t_{mid})^2 \end{bmatrix} \tag{7}$$

and W_i is the measurement noise covariance matrix. Iterating Eqs. (5) and (6) twice is sufficient to get a good estimate. The estimated covariance for $\hat{Y}$ is

$$\widehat{W} = \left[\sum_{i=1}^{m} H_i^T W_i H_i \right]^{-1} \tag{8}$$

The angles and rates are extracted from the state $\hat{Y}$ to make the fitted observation Y', which does not have the acceleration terms, $\ddot{\alpha}$ and $\ddot{\delta}$. The corresponding subset of measurement noise covariance is extracted from $\widehat{W}$ to form W'.

An orbit fit can be used for longer tracks, but the entire position and velocity state usually cannot be fully estimated, so a scaled version of the Singular Value Decomposition method [1] is used to correct only along observable component directions. The orbit estimate is used to compute the angles and their rates, α, δ, $\dot{\alpha}$, and $\dot{\delta}$. The orbit error covariance, P, is mapped to measurement space with the observation-state partials

$$W' = \tilde{H} P \tilde{H}^T, \tag{9}$$

where

$$\tilde{H} = \begin{bmatrix} \frac{\partial \alpha}{\partial x} & \frac{\partial \alpha}{\partial y} & \frac{\partial \alpha}{\partial z} & \frac{\partial \alpha}{\partial \dot{x}} & \frac{\partial \alpha}{\partial \dot{y}} & \frac{\partial \alpha}{\partial \dot{z}} \\ \frac{\partial \dot{\alpha}}{\partial x} & \frac{\partial \dot{\alpha}}{\partial y} & \frac{\partial \dot{\alpha}}{\partial z} & \frac{\partial \dot{\alpha}}{\partial \dot{x}} & \frac{\partial \dot{\alpha}}{\partial \dot{y}} & \frac{\partial \dot{\alpha}}{\partial \dot{z}} \\ \frac{\partial \delta}{\partial x} & \frac{\partial \delta}{\partial y} & \frac{\partial \delta}{\partial z} & \frac{\partial \delta}{\partial \dot{x}} & \frac{\partial \delta}{\partial \dot{y}} & \frac{\partial \delta}{\partial \dot{z}} \\ \frac{\partial \dot{\delta}}{\partial x} & \frac{\partial \dot{\delta}}{\partial y} & \frac{\partial \dot{\delta}}{\partial z} & \frac{\partial \dot{\delta}}{\partial \dot{x}} & \frac{\partial \dot{\delta}}{\partial \dot{y}} & \frac{\partial \dot{\delta}}{\partial \dot{z}} \end{bmatrix} \tag{10}$$

The key is to have a sufficiently close initial guess so the resulting angles and uncertainties are reasonable.

2.2.2 Track Association and IOD

Once the track fits are computed, they are used for correlation and track association. To perform track association and IOD for a group of n tracks, TAPIOCA converts the fitted pairs of right ascension and declination angles, (α_j, δ_j), for the first and last track in the group to line-of-sight (LOS) unit vectors $(\hat{\mathbf{o}}_j)$.

$$\hat{\mathbf{o}}_j = \begin{bmatrix} \cos\delta_j \cos\alpha_j \\ \cos\delta_j \sin\alpha_j \\ \sin\delta_j \end{bmatrix} \tag{11}$$

Using the two LOS vectors $(\hat{\mathbf{o}}_1, \hat{\mathbf{o}}_n)$, the two observer position vectors $(\mathbf{q}_1, \mathbf{q}_n)$, and the corresponding times (t_1, t_n), the object's position, $\mathbf{r}_1$, and velocity, $\mathbf{v}_1$, can be hypothesized.

The two unknowns needed to uniquely determine an orbit are the ranges at the midpoint times of the first and last track, which can be represented by the range at the initial midpoint time, ρ_1, and the average range-rate over the streak, $\bar{\dot{\rho}}$. For each combination of ranges, there exists a possible orbit solution.

Copyright © 2023 Advanced Maui Optical and Space Surveillance Technologies Conference (AMOS) – www.amostech.com

To compute the position and velocity of the spacecraft, we need the positions at the endpoints, which are

$$\mathbf{r_1} = \rho_1 \hat{\mathbf{o}}_\mathbf{1} + \mathbf{q_1} \tag{12}$$

$$\mathbf{r_2} = (\rho_1 + \Delta\rho)\hat{\mathbf{o}}_\mathbf{2} + \mathbf{q_2} \tag{13}$$

where

$$\Delta\rho = \dot{\bar{\rho}}(t_n - t_1) \tag{14}$$

With those positions and the elapsed time, a Lambert solution is obtained using Gooding's Lambert solver [2] to find the velocity at the endpoints. The challenge with using the Lambert solver is that the number of completed half-revolutions is unknown. To overcome that difficulty, a range of guesses for the number of half-revolutions are tried, from zero to a maximum determined using the elapsed time from track 1 to n and the shortest orbit period possible for the central body. To avoid excessive computation time, the maximum number of half-revolutions is limited to no more than 11, which means less than six full revolutions have ocurred.

The resulting values for $\mathbf{r_1}$ and $\mathbf{v_1}$ are used to compute the specific mechanical energy, ξ, of the orbit. If $\xi < 0$, the orbit is elliptical.

$$\xi = \frac{|\mathbf{v_1}|^2}{\mathbf{2}} - \frac{\mu}{|\mathbf{r_1}|} \tag{15}$$

We can limit the acceptable orbits to only those within an admissible region [3] defined by $\xi < 0$.

Once a hypothesized two-body orbit is produced with the Lambert solver, we want to quantify how well it matches the observed angles and rates for each fitted track with a metric, ε. We will define ε as the RMS of the Mahalanobis distances (in measurement space) for each observation computed using the two-body orbit.

$$\varepsilon = \sqrt{\frac{\sum_{j=1}^{n} y_j^T \left[W'_j\right]^{-1} y_j}{n}} \tag{16}$$

where y_j is the residual for each track fit, or Y'_j minus the observation computed from the two-body orbit. The Mahalanobis distance is a statistical measure of how well the computed observation matches the fitted observation for each track.

The smaller ε is, the better the hypothesized two-body orbit matches the observations. To find the minimum value of ε, an initial guess for range and range rate is found within the admissible region and starting with that guess, a pattern search is used to minimize ε. The pattern search involves computing ε in eight evenly spaced locations around the initial point. Note that the locations are computed using a $\Delta\rho$ and $\Delta\dot{\rho}$ with the scaling

$$\frac{\Delta\rho}{\Delta\dot{\rho}} = \frac{1000\ km}{1\ km/s} \tag{17}$$

Range rate steps are 1000 times smaller than range steps. The point with the lowest metric which is lower than the current ε is selected as the next central point and the process is repeated. If the algorithm moves in the same direction three times, the step sizes are doubled. If the algorithm does not find a lower value of ε among the eight points, the step size is halved and the process is repeated until either the step size for $\Delta\rho$ is less than 0.01 km, ε is less than 0.25, or the number of iterations is greater than 250. The three convergence criteria can be easily adjusted to tune the performance of the algorithm. The value of ε is computed for a range of half-revolutions, with the best result taken as the optimum solution.

The Lambert solution is dependent on accurate positions in space, but noise in the angles leads to error in the LOS vectors, and error in the LOS leads to error in the positions. If the angle noise is high, the Lambert solutions may not

Copyright © 2023 Advanced Maui Optical and Space Surveillance Technologies Conference (AMOS) – www.amostech.com

ever get close enough to the true orbit for the observations to match, even with perfect range hypotheses. To overcome that limitation, a final optimization is performed using a Nelder-Mead routine starting with the result from the optimum number of half-revolutions. In addition to the range and range-rate hypotheses, the two angles for both the first and last track are included in the optimized state. This allows the LOS vectors to deviate from what is observed, but not so much that they exceed the constraints imposed by the Mahalanobis distance used in computing ε.

If the final value of ε is less than a threshold (typically 7), then the group of tracks is considered a valid association. The position and velocity corresponding to the lowest value of ε is used for the initial estimate of the orbit. If the best ε is greater than 7, the group of tracks are not considered a valid association, meaning at least two different objects are represented.

2.3 TPM

The TPM service receives UCTs from CatalogCoordinator and sends them to the TPM worker services. Each TPM worker contains a different list of hypotheses, or groupings of UCTs which were successfully associated previously. The workers attempt to associate each new UCT with all the existing hypotheses. The results are sent back to the TPM service, which decides which of the possible associations is the best. Then the TPM service tells the appropriate worker to delete the old hypothesis and create a new one with the newest UCT added to the group. If a UCT does not associate to any existing hypotheses, the TPM service assigns the UCT as a one-track group to one of the workers. Each time a track is associated to an existing group, the worker checks to see if it rises to the level of a "candidate" orbit. A new candidate orbit is assigned to a worker. Before performing track association on a new UCT, the workers will first attempt to correlate the UCT to existing candidate orbits using a Mahalanobis distance in measurement space. Only if a track fails to correlate to any candidate orbits is it sent to the workers for track association. When a track correlates to a candidate orbit, the orbit is updated using batch least-squares.

When two or three tracks are being associated, the quality of the angle rate estimates is key to being able to successfully weed out false associations, or groups of tracks from more than one space object. Therefore, if such a track with a poor angle rate estimate does not associate to any candidates or existing hypotheses, it is discarded instead of being used to create a new single-track hypothesis.

2.4 Cislunar Updates

To perform track association and IOD for a variety of cislunar trajectories, modifications had to be made to TAPIOCA, TPM, and SCOPE. In TAPIOCA, the admissible region is expanded to include some "mildly" hyperbolic orbits with hyperbolic excess velocity up to 5 km/s. When doing optimization, instead of computing one initial guess, TAPIOCA computes ε over a coarse grid defined by minimum and maximum range and range-rate values and fixed intervals. Only space object positions outside of the central body and orbits with energy less than the maximum are accepted. Then local minima are computed for the grid and up to six of the best minima (lowest ε) are used as initial guesses in pattern searches to minimize ε. The value of ε is computed for every local minimum for the range of half-revolutions to determine the best solution.

In TPM, each track is evaluated to determine if it could have originated from a Moon-centered orbit. For optical tracks, the LOS vector is extended to see if it intersects the lunar Sphere of Influence (SOI), which is defined to be a radius of 66,100 km. If so, the track is labeled as possibly belonging to a Moon-centered object. When doing track association and IOD for a group of tracks, first an Earth-centered solution is attempted. If it does not pass the test as being a valid association and if at least one of the tracks in the group is a possible Moon-centered object, then a Moon-centered track association is also attempted.

In SCOPE, whenever Keplerian orbital elements are computed, the code was modified to allow for hyperbolic trajectories. When an orbit period is needed, hyperbolic orbits are given a default period of three days. Both the Earth and the Moon can be used as central bodies for orbits and they both can have spherical harmonic gravity models simultaneously. Also, eclipses are modeled for both bodies when computing solar radiation pressure.

Copyright © 2023 Advanced Maui Optical and Space Surveillance Technologies Conference (AMOS) – www.amostech.com

3. SIMULATION TESTSET

Care is taken to make the high-fidelity simulations as realistic as possible. Stressing scenarios have been incorporated into the simulations, including data gaps due to lunar brightness exclusions, formations of spacecraft in proximity, and a maneuvering satellite conducting rendezvous operations. The focus of this work is on objects near the Moon.

3.1 Force Models

NASA's General Mission Analysis Tool (GMAT) [4] is used to create the truth trajectories with high fidelity dynamic models. Objects are propagated ballistically for about 1 month with a starting date of 2019-07-20 and ending on 2019-08-22. Table 1 lists the force model parameters used to propagate the truth trajectories. Note that SCOPE uses a different propagator in the operational software. SCOPE uses the TurboProp [5] libraries for high fidelity propagation with similar force model parameters specified, thus introducing a small amount of dynamic mismodeling.

Table 1: Force model parameters

Parameter	Value
Coordinate System	Earth ICRF
Solar Radiation Pressure Area	0.012
Coefficient of Reflectivity	1.0
Gravity Field	EGM96
Gravity Potential	12 x 12
Third Body Gravity	Sun, Moon
Integrator	PrinceDormand78
Integration Accuracy	1×10^{-12}

3.2 Special Objects

Several objects are included specifically to stress the capabilities of TAPIOCA. To test the track initiation process in the presence of clustered objects a formation of three closely spaced objects (33, 34, 35) with roughly 100 km of separation is included. Given the distances involved and the measurement noise applied TAPIOCA will struggle to discern the individual objects. No a priori information is provided to the system, hence there is a high chance of associating tracks from all three objects in the cluster.

A maneuvering object that is performing rendezvous is included. Object 36 begins near the cluster mentioned above (33, 34, 35), then 14 days into the simulation it performs a 0.155 km/s maneuver to enter a transfer trajectory. After 4 days a second 0.124 km/s maneuver is performed to match trajectories with an HN1-100 orbit. SCOPE does have maneuver detection capabilities; however, they are not utilized in this study. Lacking a maneuver detection capability, one would expect that the object will be lost after a maneuver of sufficient magnitude is performed. The desired outcome is that TAPIOCA will pick the object back up by forming a new solution based on the UCTs coming from object 36 once on its new trajectory.

3.3 Trajectories

The simulated data includes 30 objects in various cislunar orbits. Table 2 describes each of the orbits included. Originally the set included 48 objects, hence the numbering in the table. Eighteen objects were removed for this study to decrease computation times. The objects chosen for removal are not challenging for SCOPE to handle. For more information on the cislunar family and orbit number definitions see [6]. A visualization of the objects from Earth in RA and DEC from the Moon is presented in Figure 2. The objects start at the simulation epoch and include 2 days of propagated trajectory.

Copyright © 2023 Advanced Maui Optical and Space Surveillance Technologies Conference (AMOS) – www.amostech.com

Table 2: List of simulated object trajectories

Object	Cislunar family	Orbit numbers	comment
1, 3	HN1	100	Halo objects in same orbit separated in phase
11-13	HN1	50, 100, 150	Constellation of 3 halo objects starting at same phase in same family (Note: orbits 1, 3 and 12 form a cluster of 3 halo objects separated by ~1000 km)
14-16	HS1	50, 100, 150	Constellation of 3 halo objects starting at same phase in same family
17-19	HN2	50, 100, 150	Constellation of 3 halo objects starting at same phase in same family
20-22	HS2	50, 100, 150	Constellation of 3 halo objects starting at same phase in same family
33-35	HN1	200	Cluster of 3 halo objects separated by ~100 km
36	HN1	200→100	Maneuvering object that starts in vicinity of objects 33-35 cluster and ends at HN1-100 orbit after 4-day transfer
37-39	L1	50, 100, 150	Constellation of 3 Lyapunov objects starting at same phase in same family
40-42	L2	50, 100, 150	Constellation of 3 Lyapunov objects starting at same phase in same family
43	A1	50	Axial family object that remains in same lunar vicinity as previous objects
44	A2	50	Axial family object that remains in same lunar vicinity as previous objects
45-46	V1	50, 100	Vertical family objects that remain in same lunar vicinity as previous objects
47-48	V2	50, 100	Vertical family objects that remain in same lunar vicinity as previous objects

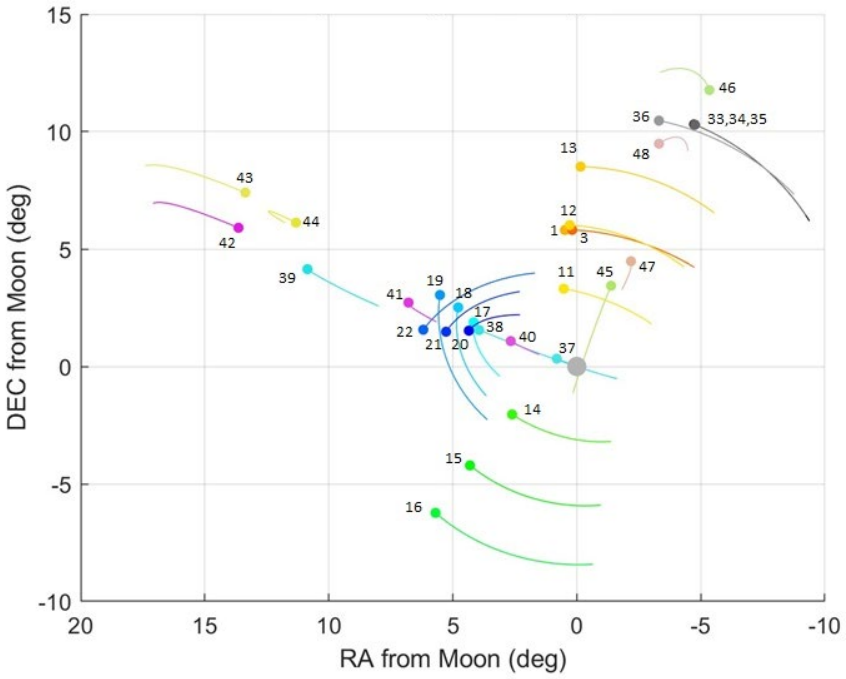

Figure 2: Display of the positions of the orbits with lines representing two days of the trajectory propagation, in right ascension and declination as viewed from center of Earth.

Copyright © 2023 Advanced Maui Optical and Space Surveillance Technologies Conference (AMOS) – www.amostech.com

3.4 Measurements

Optical observations of right ascension and declination are generated using an Earth ground-based electrooptic sensors (EO-ground). A set of five longitudinally distributed sensors are used to ensure the cislunar regime is continuously visible from at least one of the sites. Table 3 provides the site locations.

Table 3: Ground sites provided EO observations.

Site	(Latitude, Longitude)
New Mexico	(33.8° N, 106.7° W)
Maui	(20.7° N, 156.3° W)
Diego Garcia	(-7.4° N, 72.5° E)
Spain	(37.1° N, 5.6° W)
Australia	(-21.9° S, 114.1° E)

Tasking of observations is done on a sensor-by-sensor basis where the object with the longest gap in time since its last observation from a particular sensor and currently observable by that sensor is selected. For Earth-based EO observations exclusion zones are included: objects are at least 10 degrees above the horizon, the Sun is at least 10 degrees below the horizon, the object is at least 1 degree from the Moon, and the object is brighter than 24 magnitude (where the object is modeled as a diffuse sphere with 1 m^2 cross-sectional area and reflectance of 20%).

Once selected, the object is observed N times with a Δt time gap between each observation to form a track. For EO observations, other objects within 0.1 degrees of the targeted object are also observed simultaneously and if any of the objects are within 0.2 arcsecs of one another, the observations are combined by averaging and a single RA/DEC is reported for that observation. In the baseline scenario, tracks had $N = 5$ observations with $\Delta t = 60$ sec spacing, giving a 4-minute track as displayed in Figure 3.

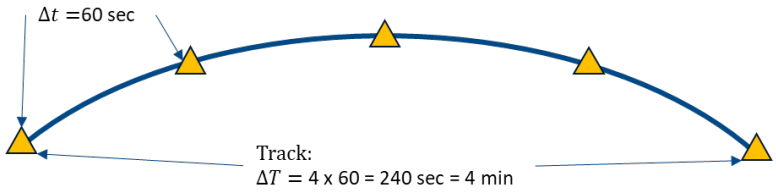

Figure 3: Visualization of track definition

Pristine observations are generated initially, and varying levels of random noise are added during the analysis. In addition to the exclusions and tasking priority listed above, 60 sec are allotted between observations to simulate sensor downtime due to re-positioning and acquisition.

Figure 4 shows the observation times of each track for each object in the baseline case. The different ground sensors are displayed in different colors. The gap in observations around day 10 of the simulation corresponds to new Moon when all the objects are visibly close to the Sun. This gap lasts for roughly 5-7 days (depending on the object orbit) and causes difficulties maintaining track custody in the estimator.

Copyright © 2023 Advanced Maui Optical and Space Surveillance Technologies Conference (AMOS) – www.amostech.com

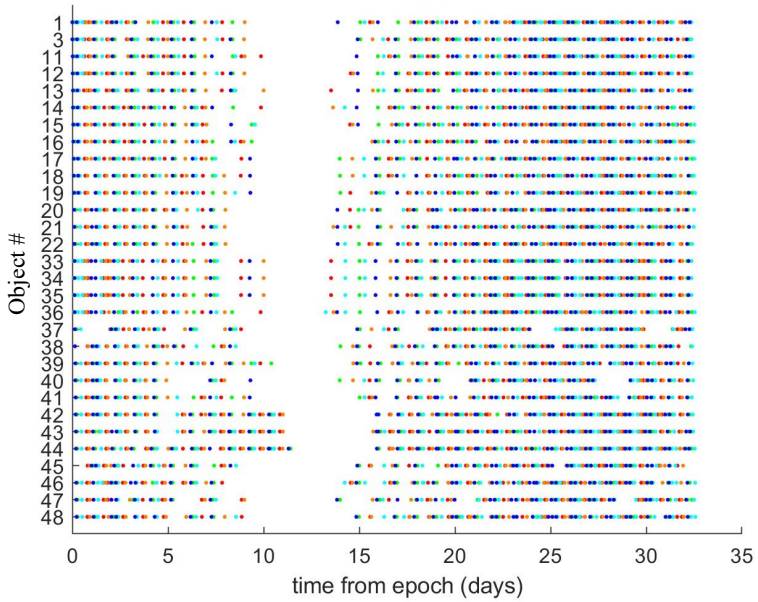

Figure 4: Depiction of times of each track generated for each object. Different colors represent ground sites.

4. RESULTS

This section presents the results of testing SCOPE with a parameter search of track length, track cadence, and measurement noise. Section 4.1 introduces the baseline scenario and the parameters varied in this study. In total 45 simulations are run. Given the size of the simulation, a thorough investigation of each run is not feasible. However, to understand the high-level results better, a deep dive into the baseline run is presented in Section 4.2. Results and statistics from the parameter search are presented in Section 4.3.

4.1 Parameter Search

To test the capabilities of the cislunar IOD code, numerous simulations are run with varying parameters, specifically the total number of tracks, track length, and measurement noise. A baseline is chosen as a starting point. The baseline scenario has 4520 total tracks over 32 days with 4-minute track lengths consisting of 5 observations within a track, and 1 arcsec of measurement noise (1σ Gaussian) on each observation. The scenario has a high cadence of tracking data, representing a dedicated cislunar cataloging effort.

The baseline is realistic in its track length (4 min) and noise (1 arcsec) considering current sensor capabilities. Raven class sensors can produce measurements at these levels. Less realistic is the large number of observations. Given the current number of objects in space and the low number of those is cislunar regions, there is currently minimal demand for dedicated monitoring. Case 1 has a total of 4520 tracks, which amounts to ~ 140 tracks per night or ~ 28 tracks per sensor per night. The average tracks per object per night is ~ 4.7. Given that the IOD process requires at least 5 associated tracks to create a candidate, one could be formed with one night of tracking data. From this baseline the track length is varied by a factor of 10 in both directions, for tracks of length 0.4 min (24 sec) and 40 min. The noise is varied from the baseline by a factor of 2 in both directions twice. Measurement noise varied from 0.25 arcsec to 4 arcsec.

Three cases are studied, decreasing the total number of tracks produced in each to represent a more realistic track generation cadence based on current sensor scheduling demands. Case 2 has half the number of tracks as Case 1, and Case 3 has a quarter of the tracks. In Case 3 the average tracks per object per day is only 1.2, hence the expectation is that it will take at best ~ 4 nights to generate a candidate. Table 4 provides a summary of the three cases for comparison. Each case has 15 runs for a grand total of 45 runs.

Copyright © 2023 Advanced Maui Optical and Space Surveillance Technologies Conference (AMOS) – www.amostech.com

Table 4: Parameters varied for each case. Parameters in bold are the baseline values.

Case	Track Lengths	Track cadence	Noise (arcsec)	Total Tracks	Tracks/object/day
1	0.4 min / **4 min** / 40 min	**10 min**	0.25, 0.5, **1**, 2, 4	**4520**	**4.7**
2	0.4 min / 4 min / 40 min	20 min	0.25, 0.5, 1, 2, 4	2272	2.4
3	0.4 min / 4 min / 40 min	40 min	0.25, 0.5, 1, 2, 4	1141	1.2

Some considerations to note. Short tracks can be difficult and problematic. While ideal for generating more measurements, there is a tradeoff. Cislunar objects tend to be dim and require longer integration times to produce better signals for detection in the image. Hence, short tracks could lead to a higher chance of missing a detection. Also, a key part of the IOD process as implemented is an estimate of the angular rates, which can be significantly influenced by measurement noise when the track length is short. Longer tracks are generally better and in line with data available from the Planetary Defense Coordination Office. To maintain consistency when comparing runs within a case, the number of tracks is kept constant for all runs in the case.

4.2 Baseline Results

This section will present some in-depth results from a simulation run on the baseline scenario. Only the high-level results and statistics from runs varying the parameters are presented in the next section. This in-depth analysis is provided so that the high-level results can be more easily interpreted.

The baseline scenario is bolded in Table 4. The total number of tracks is 4520, with an average of 151 tracks per object. Over 32 days of simulation that amounts to 4.7 tracks/object/night. Random Gaussian noise with a sigma value of 1 arcsec is added to the observations. The run took 2.2 hours to complete on a server with 24 compute threads.

There are 30 objects in the simulation. Since object 36 performs two maneuvers, and maneuver detection and handling are not considered in this work, it is expected to be lost and re-found twice. The best-case scenario would be finding 32 candidates and subsequent graduates representing the 30 objects found once and the maneuvering object found two additional times. The baseline run found 34 candidates and 33 graduates. The maneuvering object is indeed found twice. It is lost on Aug-07, re-found on Aug-10 only to be lost on Aug-11, then re-found the second time on Aug-13. A false candidate is formed for object 34, using tracks from object 33 and 34, but it never achieved the threshold for graduation. One object (38) is lost on Jul-29 due to the gap in observations caused by the Sun. It is re-found on Aug-5. Following are the association and correlation statistics:

Association Statistics:
Number of true positive associations = 201
Number of false positive associations = 136
Number of true negative associations = 3945
Number of false negative associations = 7

Correlation Statistics:
11.33% Observations not correlated.
88.67% Observations correlated.

Estimated objects are compared against the set of truth trajectories to find the closest match and validate the results. Figure 5 shows the natural log of the distances between each estimated object position and the truth trajectories after processing the last observation for each estimate. Dark blue represents a small difference, typically ~ 1 km, between the estimated position and the true position. This plot highlights the proximity of some of the objects. The matrix excerpt shows the final distances between the clustered objects 33, 34, and 35. The object that is lost but re-found is clearly seen, as well as the effects of the maneuvering object. Objects 1, 3, and 12 are also close to each other. The mean final error of all the objects, including objects lost, after their last processed observations is 1.1 km. Considering only objects that are present on the last day of the simulation, the mean final errors are 0.69 km.

Copyright © 2023 Advanced Maui Optical and Space Surveillance Technologies Conference (AMOS) – www.amostech.com

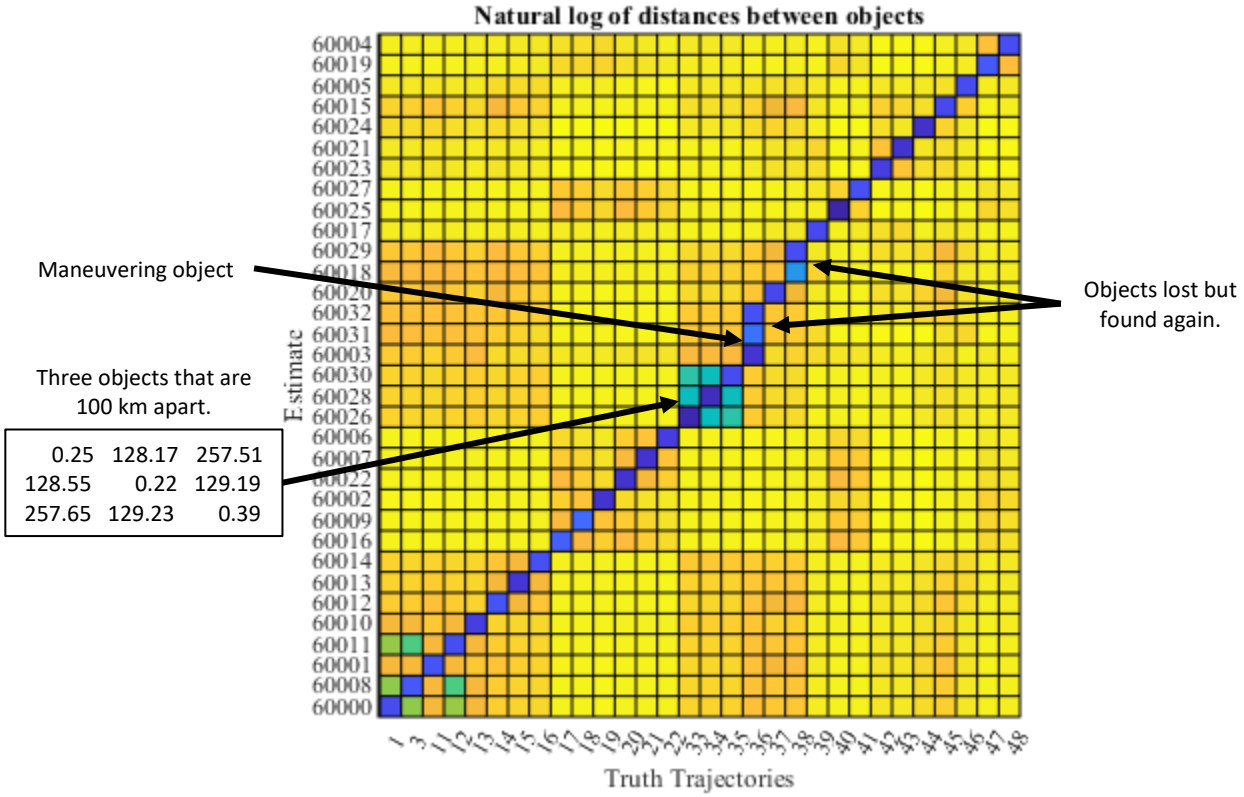

Figure 5: Distances at final time between each estimate position state with the truth trajectories.

Table 5 presents statistics on the IOD process. While the best-case scenario is that candidate creation occurs on the 5th track, that is not always the case if the tracks don't associate well. Sixteen candidates are created based on the first 5 tracks processed. In this run it took 5-6 tracks to create most candidates. The slowest candidate creation is on the 48th track processed, which arrived 15.8 days into the simulation, for object 35. These results indicate the difficulties that can arise due to clustered objects (33, 34, 35).

Table 5: Candidate and Graduate statistics.

	Median creation time	Mean creation time	Mean position error	Mean position 1-σ uncertainty
Candidate	0.69 days on 6th track	1.57 days	67.9 km	70.3 km
Graduate	2.0 days on 13th track	2.62 days	19.4 km	40.3 km

Next is a deeper investigation into the behavior of the objects, specifically two objects which are representative of the population. Figure 6 displays the position and velocity RSS errors of the estimates for object 3 and 20. Subplots 1 and 3 show the position and velocity errors respectively in blue with the 2σ uncertainty values in red. For object 3 the IOD solution computed by TAPIOCA has ~75 km of 2σ uncertainty in position that is reduced over the course of 7 days. The data gap due to the Sun starts on 29-Jul and lasts for 5.9 days in which there are no tracks. The data gap can be seen where the 2σ uncertainty grows to over 100 km. Once tracks are produced again on 04-Aug the filter quickly corrects the estimate. It can be difficult to see trends in the position/uncertainty plots, so the Mahalanobis values for position and velocity are displayed in subplots 2 and 4. The red line is the critical value: the square root of the inverse cumulative chi-square distribution function with 3 degrees of freedom evaluated at the 0.997 probability value. The Mahalanobis value can be more insightful as it will better capture whether the errors are surpassing the uncertainty bounds in a particular dimension, whereas the RSS position/velocity plots could mask that information if the errors/uncertainties are large in one dimension and small in another. The code is set to output a prediction for several days past the last track. In this case the last track for object 3 is on 21-Aug, hence the growth in the errors and uncertainties after that date. Object 20 shows the same general trends as do most of the population.

Copyright © 2023 Advanced Maui Optical and Space Surveillance Technologies Conference (AMOS) – www.amostech.com

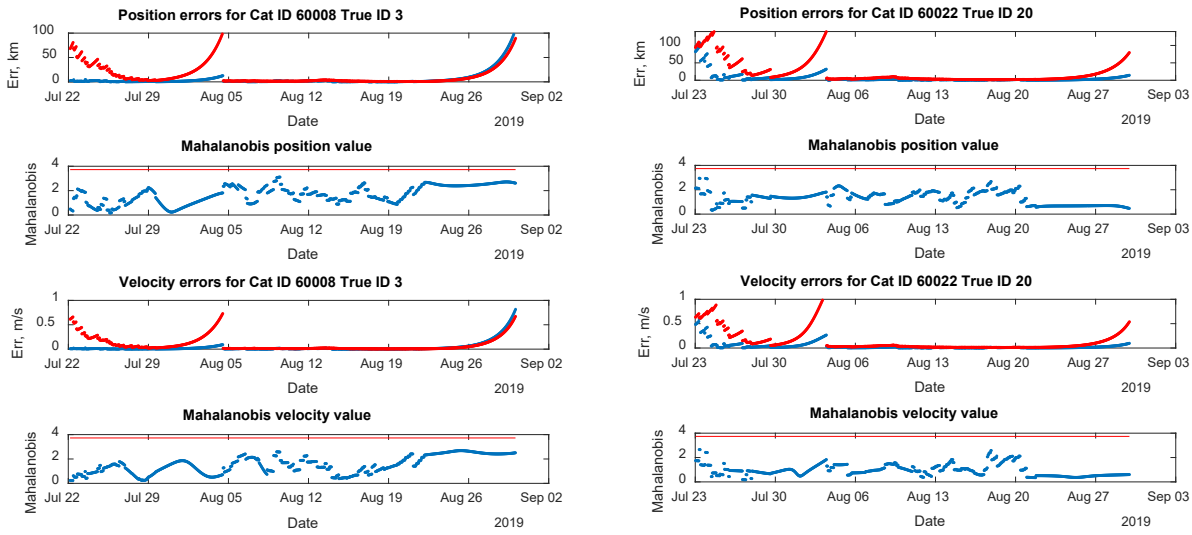

Figure 6: Error plots for True ID 3 left and True ID 20 right. Subplots 1 and 3 show the position and velocity errors in blue with 2σ uncertainties in red. Subplots 2 and 4 show the corresponding Mahalanobis value in blue relative to the critical value in red.

All the objects show the same general trends regarding initial uncertainty reduction, error/uncertainty growth during the data gap and at the end of the simulation. If the state errors are too large when the data gap occurs the estimated object error could grow to the point that it no longer correlates to incoming measurements and is lost. In this run that happened to object 38. Figure 7 presents the error plots for the two estimates found from object 38 data, with the pre-gap estimate 60018 on the left and the post-gap estimate 60029 on the right. Objects can be lost more often when the measurement noise is larger, among other causes. After the data gap, as tracks for 38 are processed and not correlated to any objects, the tracks are tagged as UCTs and sent to TAPIOCA. Candidate 38 is re-found after the first 6 tracks are collected post-gap on 05-Aug-2019 about 7.6 days after the last track pre-gap.

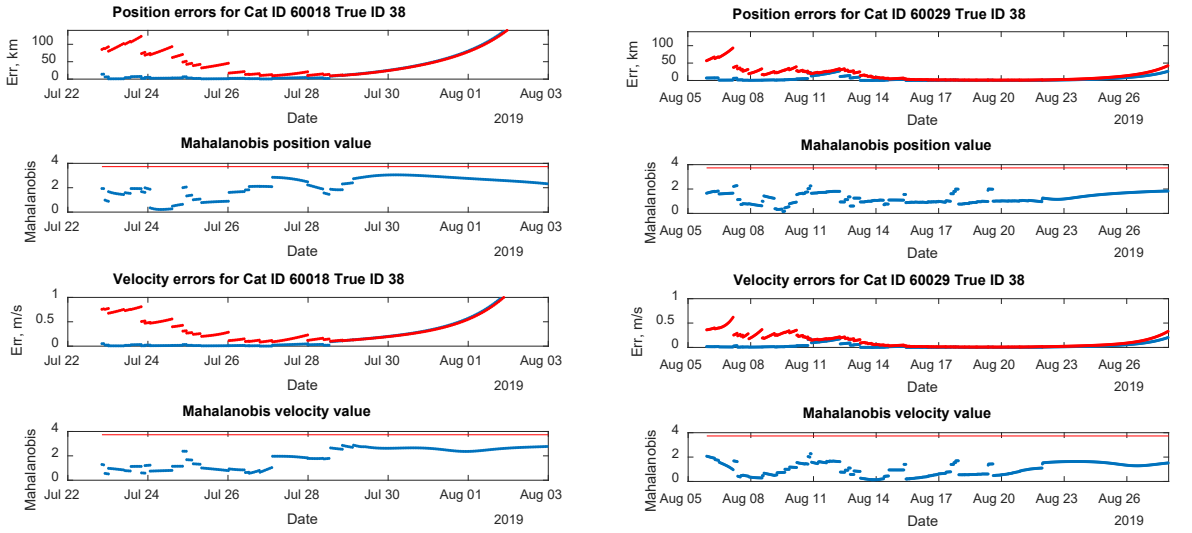

Figure 7: Error plots for True ID 38, showing pre-gap on left and post-gap on right. Subplots 1 and 3 show the position and velocity errors in blue with 2σ uncertainties in red. Subplots 2 and 4 show the corresponding Mahalanobis value in blue relative to the critical value in red.

Copyright © 2023 Advanced Maui Optical and Space Surveillance Technologies Conference (AMOS) – www.amostech.com

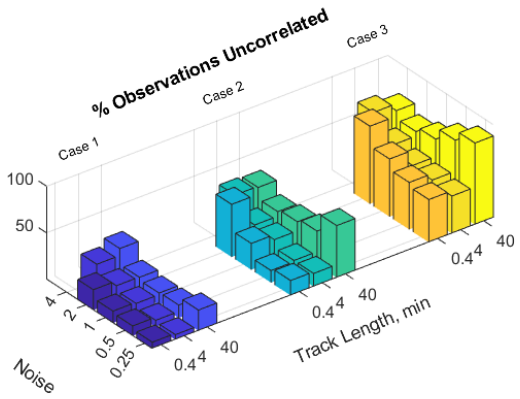

Figure 8: Chart comparing the percentage of observations that were not correlated to an estimate.

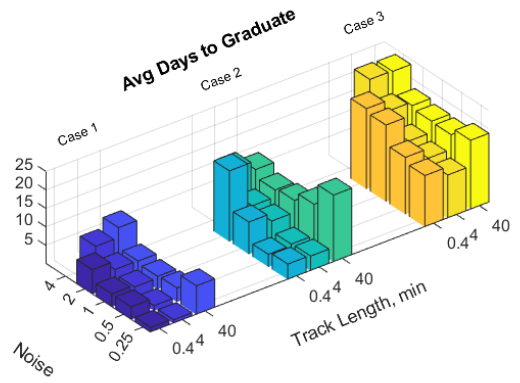

Figure 9: Chart comparing the average number of days that it took to graduate objects in SCOPE.

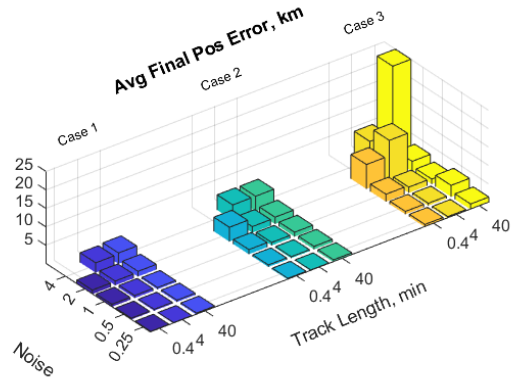

Figure 10: Chart comparing the average final position errors of the estimates after the last measurement.

4.3 Parameter search results

With the insights into a single run from the previous section as a reference, this section explores the overall statistics from all the runs. Given the size and complexity of the simulation, there is a wealth of data that could be presented. Three outputs are particularly useful to gauge the overall effectiveness of the cislunar IOD. First is the percentage of observations that are correlated to estimated objects presented in Figure 8. This percentage does not include UCTs that go unused, and those that are used to form candidates. Locating high quality candidates quickly will keep this percentage low. High percentages of uncorrelated observations indicate poor IOD and/or predictions of estimates. The second output is the average number of days required to graduate objects as presented in Figure 9. A timer is initiated at the beginning of the simulation and recorded when an estimate graduates. When an estimate is lost, the timer is re-started after the last track is correlated and recorded when the estimate graduates again. A side effect of this method of recording the times causes the average days to graduate to be biased toward larger values when estimates are lost due to the gap in observations from the solar exclusions. The third output is the average final position error of the estimates relative to the truth trajectories after the last track is processed as presented in Figure 10. In some instances, this value can be difficult to interpret. For example, consider a case where several estimates are so poor that they are lost, the errors from those objects will not affect the average, whereas if those poor estimates are considered their errors could significantly increase the average error.

Figures 8-10 present the results of the 45 runs as bar charts to highlight trends in the data. The x-axis represents the track length of 0.4, 4, and 40 minutes, separated into groups for the three cases, which are labeled under the title. The y-axis represents the measurement noise that is applied. Some bars are missing from the charts, specifically the results for short tracks with large noise (0.4 min tracks with 4 arcsec noise). These runs did not process successfully because the angle-rate estimates had too much error. Finally, the z-axis represents the output detailed in the title of the figure.

As expected, the results get worse (larger output in each figure) as the total number of tracks is reduced. As a reminder Case 1 had 4520 total tracks, Case 2 had 2272 total tracks and Case 3 had 1141 total tracks. Another expected result is that the average final errors are strongly correlated with the measurement noise present as seen in Figure 10.

A less intuitive trend appears in Figures 8 and 9, most clearly in Cases 2 and 3 of Figure 8 and Case 2 of Figure 9, where worse results appear at the extremes of higher

Copyright © 2023 Advanced Maui Optical and Space Surveillance Technologies Conference (AMOS) – www.amostech.com

noise with shorter tracks and lower noise with longer tracks. These trends are a result of estimating the angular rates in the IOD process. Angular rate estimates from shorter tracks are more sensitive to measurement errors. Large measurement errors can lead to very poor rate estimates, which can lead to poor associations and IOD results. Hence the greater number of days needed to graduate estimates. This is a difficult problem to overcome. At the other extreme, longer tracks allow for more accurate angular rate estimates, which is also captured in the estimated rate uncertainty value. However, the error in the two-body approximation, when mapped into angular rate uncertainty for associating with the measurements, can become larger than the small rate uncertainty and lead to track associations being rejected. There may be room for improving the algorithm to better handle this situation.

The average position errors of the objects at the end of the simulation in Figure 9 are very good. Generally, when the measurement noise is 1 arcsec or better the final average errors are under 1 kilometer. The major exception is in Case 3 where there are not enough tracks to form good estimates. When only 1-2 tracks are available per night the measurement error becomes a major consideration.

Accurate state estimates are critical given the chaotic dynamics of the 3-body system, where large errors in position can grow quickly when predicting the next contact opportunity days into the future.

Table 6 presents the data on each run presented in Figures 7-9 as well as other output. In good runs each candidate is graduated, however when the measurement noise is too large an excessive number of candidates are created. Typically, only robust estimates are graduated, hence there is less fluctuation in the number of graduates. In the table the percentage of observations correlated is listed (versus the percentage of observations uncorrelated as in Figure 8). The best run correlated 94.7% of the observations (case 1, 4 min, 0.25 arcsec), while the worst run correlated 12.6% (case 3, 40 min, 0.25 arcsec).

The columns labeled ‘False Neg’ and ‘False Pos’ refer to the count of False Negative associations and False Positive associations respectively. A high count of false negative associations implies associations are being missed, and generally correlates with degraded performance.

There is a less clear connection between false positive association counts and performance. Shorter tracks result in worse angular rate estimates, which is captured as higher uncertainties for the rate estimates. Thus, the algorithm will accept more associations due to the higher uncertainty, resulting in a higher false positive association rate. Whereas for longer tracks, the angular rate estimates are better, since any noise in the angle measurements has a smaller effect. However, that means the uncertainty is smaller which causes the algorithm to make less associations because it has much lower tolerances for matching noisy measurements to approximate two-body orbits.

The column ‘Moon Cand’ indicates how many of the candidates are formed using the Moon as the central body instead of the Earth. Longer track lengths tended to cause the algorithm to utilize the Moon, and it occurs more frequently when the cadence of tracks is lower. The results tended to be better when most estimates are formed using Earth as the central body. Future work should include more Lunar centric objects to test that it is utilized when appropriate. An interesting note is that a high count of Lunar centric candidates did not greatly impact the overall performance as seen in case 1, with 40-minute track lengths.

The column ‘Lost Count’ refers to how many objects are missing at the end of the simulation. The data rich environment of case 1 always had all 30 objects present at the end of the simulation. As expected, less tracks present in case 3 led to a significant number of objects being lost or never found. Of particular note is that the cluster of objects (33, 34, 35) are lost or never found in several of the runs. The column ‘Multiples Count’ refers to the number of objects that had multiple candidates found. In the perfect run there is at least one multiple due to the maneuvering object 36. Generally, there are several multiples due to the data gap.

Copyright © 2023 Advanced Maui Optical and Space Surveillance Technologies Conference (AMOS) – www.amostech.com

Table 6: Results from all runs. (m) indicates the maneuvering object was not found for each segment of its trajectory. (c) indicates that the cluster (33, 34, 35) of objects was lost at simulation end.

Run	Cands #	Grads #	Corr %	False Neg	False Pos	Moon Cand	Avg Err km	Lost Count	Multiples Count	Grad Days
CASE 1 – 4520 Tracks										
0.4 min Track										
0.25 arcsec	32	32	93.3	0	109	3	0.24	0	1	1.3
0.5 arcsec	33	33	89.6	6	212	3	0.36	0	2	3.4
1 arcsec	35	33	87.4	10	137	3	0.7	0	4	3.5
2 arcsec	34	34	78.2	5	287	4	1.1	0	3	6.6
4 arcsec	-	-	-	-	-	-	-	-	-	-
4 min Track										
0.25 arcsec	32	32	94.7	5	6	4	0.23	0	1	1
0.5 arcsec	32	32	93.0	6	58	2	0.39	0	1	1.4
1 arcsec	34	33	88.7	7	136	4	0.69	0	3	3
2 arcsec	34	33	83.4	9	112	1	1.17	0	3	4.3
4 arcsec	56	38	74.2	18	139	3	2.66	0	15	7.1
40 min Track										
0.25 arcsec	31	31	77.8	3811	2	23	0.44	0	1 (m)	7.8
0.5 arcsec	32	32	86.2	1448	5	23	0.49	0	1	3.8
1 arcsec	33	32	87.0	456	1	13	0.47	0	2	3.5
2 arcsec	34	33	83.9	19	4	7	1.42	0	3	4.2
4 arcsec	79	40	66.8	65	133	14	2.96	0	20	9.8
CASE 2 – 2272 Tracks										
0.4 min Track										
0.25 arcsec	34	33	84.1	6	169	6	0.35	0	3	4.2
0.5 arcsec	34	34	87.1	5	78	4	0.54	0	3	3.4
1 arcsec	38	37	71.8	7	353	3	1.26	0	7	8.7
2 arcsec	39	31	43.7	9	603	5	3.85	1	6 (m)	19.1
4 arcsec	-	-	-	-	-	-	-	-	-	-
4 min Track										
0.25 arcsec	32	32	86	101	54	16	0.24	0	2 (m)	4
0.5 arcsec	35	35	85.8	15	65	7	0.39	0	4	3.8
1 arcsec	38	38	77.2	25	160	7	0.82	0	7	6.6
2 arcsec	41	37	75.2	13	71	9	1.66	0	10	7.3
4 arcsec	59	36	56.9	27	239	8	4.1	0	17	13.7
40 min Track										
0.25 arcsec	31	29	44.2	2582	6	23	0.63	3	3 (m)	18.1
0.5 arcsec	34	33	63.8	1304	24	28	0.82	0	4 (m)	12.2
1 arcsec	34	33	67.5	618	93	25	1.21	1	4 (m)	9.8
2 arcsec	43	36	70.4	203	99	29	1.85	0	11 (m)	9.2
4 arcsec	61	38	58.2	82	216	16	4.08	1	17	11.3
CASE 3 – 1141 Tracks										
0.4 min Track										
0.25 arcsec	38	30	54.2	17	255	12	0.7	3 (c)	10 (m)	13.9
0.5 arcsec	39	29	49.6	21	301	9	0.8	3 (c)	12 (m)	15.4
1 arcsec	35	30	38.2	12	410	8	2	1	5 (m)	20.7
2 arcsec	22	16	16.8	2	507	3	6.6	15	3 (m)	21.7
4 arcsec	-	-	-	-	-	-	-	-	-	-
4 min Track										
0.25 arcsec	44	32	59.9	78	103	21	0.46	2	13 (m)	11.7
0.5 arcsec	44	31	56.5	43	139	20	0.63	3	15 (m)	12.8
1 arcsec	47	33	54.6	42	112	17	1.55	2	13 (m)	14
2 arcsec	47	32	46.3	35	212	19	10.76	0	13 (m)	18.8
4 arcsec	46	22	25.3	37	405	8	7.04	8	16	23.8
40 min Track										
0.25 arcsec	11	8	12.6	1044	9	4	1.49	22	1 (m)	18.7
0.5 arcsec	25	19	23.3	778	19	13	3.09	14	7 (m)	16.8
1 arcsec	39	29	35.9	392	39	21	1.37	6	13 (m)	17
2 arcsec	47	31	41.5	154	106	20	2.73	3 (c)	18 (m)	17.8
4 arcsec	64	27	32.8	100	143	26	25.09	3	24	23.6

Copyright © 2023 Advanced Maui Optical and Space Surveillance Technologies Conference (AMOS) – www.amostech.com

5. DISCUSSION

KBR's TAPIOCA tool was successfully applied to a realistic high-fidelity simulation cataloging cislunar objects. Through a parameter search varying the total tracks, track lengths, and measurement noise the robustness of the tool was validated. Uncorrelated tracks are correctly associated to find valid estimated states that can seed a catalog maintenance algorithm with as few as 5 tracks. The limitation on track lengths was explored and objects could be found with short < 1 min tracks up to 40-minute-long tracks. Objects lost due to data gaps or maneuvers are quickly re-found. Errors in the estimated states are less than 4 kilometers except in challenging scenarios. Objects can be found and maintained when as little as 1-2 tracks are available per night.

Performance degradation does start to occur in the edge cases explored, i.e. noisy short tracks or precise long tracks. An issue which was not addressed in the results is the processing time required. When performance starts to degrade the runtimes grow quickly. Edge cases that produce too many false positive associations suffer longer run times as the numerous associations lead to a combinatorics explosion. On the other hand, too few associations due to high counts of false negative associations will delay finding candidates to graduate which also leads to longer runtimes. These issues will be investigated and managed in future code updates. Processing times were reasonable for the majority of the runs, which took between 1 to 4 hours. While the runtimes seem long, the code was processing 1,000 – 4,000 tracks over 32 days, propagating 30+ objects with no a priori information.

Considerations that can guide future work include an in-depth study of acceptable a priori position tolerances for future state predictions in the cislunar regime. The average final errors ranged between 1-4 km for many runs. Clearly these errors do not burden the catalog process when tracks are processed within 1-3 days. However, the data gap present in this study, which was 5-7 days long, did cause many estimates to be lost due to poor predictions. Future research using observations of actual cislunar objects is also planned.

6. ACKNOWLEDGEMENTS

This work was funded by the Air Force Research Laboratory under contract FA9453-18-C-0035.

References

[1] R. P. Russel and M. Lara, "Repeat Ground Track Lunar Orbits in the Full-Potential Plus Third-Body Problem," in *AIAA/AAS Astrodynamics Specialist Conference*, Keystone, CO, 2006.

[2] R. Gooding, "A Procedure for the Solution of Lambert's Orbital Boundary-Value Problem," *Celestial Mechanics and Dynamical Astronomy,* vol. 48, pp. 145-165, 1990.

[3] A. Milani, "The Asteroid Identification Problem. I. Recovery of Lost Asteroids," *Icarus,* vol. 137, no. 2, pp. 269-292, 1999.

[4] The GMAT Development Team, "General Mission Analysis Tool (GMAT)," 2022. [Online]. Available: https://gmat.sourceforge.net/doc/R2022a/html/index.html. [Accessed 2023].

[5] K. Hill and J. Gutierrez, "TurboProp C++ Mathematical Specification," KBR NTG, 2023.

[6] C. Chow, C. Wetterer, K. Hill, C. Gilbert, D. Buehler and J. Frith, "Cislunar Periodic Orbit Families and Expected Observational Features," in *The Advanced Maui Optical and Space Surveillance Technologies (AMOS) Conference*, Maui, HI, Sept 15-18, 2020.

[7] K. Hill, "Maneuver Detection and Estimation with Optical Tracklets," in *Advanced Maui Optical and Space Surveillance Technologies (AMOS) Conference*, Maui, HI, September 2014.

Copyright © 2023 Advanced Maui Optical and Space Surveillance Technologies Conference (AMOS) – www.amostech.com